Analyst

RSC Publishing

PAPER

View Article Online
View Journal | View Issue

Cite this: *Analyst*, 2013, **138**, 3463

Ultrasensitive electrochemiluminescence detection of lengthy DNA molecules based on dual signal amplification†

Fang Liu,‡[a] Heng Liu,‡[b] Meng Zhang,[a] Jinghua Yu,*[a] Shaowei Wang[a] and Juanjuan Lu[a]

Aimed at the facile detection of lengthy DNA molecules, an easily operated sandwich-type electrochemiluminescence (ECL) DNA biosensor was constructed on a glassy carbon electrode (GCE) based on CdTe quantum dots coated hollow ZnO nanoparticles (CdTe–ZnO NPs)–$S_2O_8^{2-}$ ECL system in this work. To fabricate a high-performance protocol, the GCE surface was successively modified by graphene nanosheet (GS), carbon nanotube (CNT) and gold nanoparticles (AuNPs) to form AuNPs dotted CNT–GS composites (Au@CNT–GS) platform, which improved the electronic transmission rate as well as increased the amount of immobilized capture probe CMV-F (S_1). For further ultrasensitive, stable and low-potential ECL detection, CdTe–ZnO NPs were synthesized, and employed to label signal probe T7 promoter (S_3). Based on the hybridization effect, the immobilized capture probe S_1, target DNA and labeled signal probe S_3 formed a sandwich-type DNA complex, which produced the ECL emission in the presence with $S_2O_8^{2-}$ coreactant. Under optimal conditions, the DNA ECL biosensor showed a good linear range over 10^{-14} M to 10^{-19} M with a low detection limit of 0.61×10^{-19} M. The proposed strategy demonstrates a reproducible, stable, and potent method that can be expanded to detect the genome which exists in living cells.

Received 6th March 2013
Accepted 2nd April 2013

DOI: 10.1039/c3an00452j

www.rsc.org/analyst

1 Introduction

The specific sequence detection of DNA has attracted considerable interest due to its broad applications in molecular diagnostics, genetic therapy and early screening of diseases.[1,2] Numerous analytical systems[3–5] have been developed for the detection of DNA sequences and so far, research has mainly focused on short DNA sequences (dozens of base pairs) detection. However, the DNA strands relevant to disease existing in organisms are usually more than five thousand base pairs long. Therefore, a facile and sensitive biosensor for lengthy DNA strands is urgently needed. The lengthy DNA strands researched here were obtained by cutting EGFP gene at Hind III site. The DNA strands contain a coding sequence which corresponds to human codon-usage preferences. Electrochemiluminescence (ECL), which has excellent sensitivity, wide dynamic concentration response range of chemiluminescence and high selectivity of electrochemistry, has been widely used in many fields.[6–8] By employing ECL-active species as labels on biological molecules, including antibody, antigen and DNA strands, ECL has found application in immunoassays and DNA analyses.[9–11] It can be anticipated that ECL will be capable of sensitive detection of lengthy DNA strands.

In recent years, quantum dots (QDs) have generated great research interest due to unique luminescent properties and relatively low cost for preparation. However, relatively fewer detection applications have been reported concerning the QDs ECL, though ECL analysis has many advantages over photoluminescence due to the absence of background from unselective photoexcitation. The reasons are partly that the ECL of QDs is weaker than that of conventional luminescent reagents such as luminol or $Ru(bpy)_3^{2+}$, and that QDs ECL with a high excited electrochemical potential are unstable. Thus, it is significant to modify the QDs or prepare QDs derivatives to obtain an intensity-enhanced ECL and a lower applied potential. Recently, Zhu utilized the wide band gap of zinc oxide (ZnO) to synthesize ZnO–CdS composite, which showed higher ECL intensity, lower applied potential and better stability[12] than CdS QDs. Similarly, hollow ZnO nanoparticles (ZnO NPs) were used in this paper to load more CdTe QDs as well as to modify CdTe QDs (named CdTe–ZnO nanocomposites).

To perform as an excellent sandwich-type DNA biosensor, stability and activity of the immobilized DNA strands on

[a]Key Laboratory of Chemical Sensing & Analysis in Universities of Shandong (University of Jinan), School of Chemistry and Chemical Engineering, University of Jinan, Jinan 250022, P. R. China. E-mail: ujn.yujh@gmail.com; Tel: +86-531-82767161

[b]Ministry of Health Key Lab for Otolaryngology, Qilu Hospital of Shandong University, Jinan 250012, P. R. China

† Electronic supplementary information (ESI) available. See DOI: 10.1039/c3an00452j

‡ These authors contributed equally to this work.

platform have been a longstanding goal.[13–16] Various nanomaterials have been employed to modify the biosensing platform, aimed at improving the sensing performance including electron transportation, high thermal conductivity, excellent mechanical stiffness and good biocompatibility, and this modified platform shows promising applications. Graphene nanosheet (GS) and gold nanoparticles (AuNPs) have rapidly gained interest owing to their remarkable properties, such as great mechanical strength,[17] excellent thermal,[18] good biocompatibility[19] and electrical conductivity.[20] Therefore, graphene or graphene-based materials hold great promise for applications requiring fast electron transfer, such as ECL.[21] Carbon nanotube (CNT) composites or multilayers have attracted much attention in nucleic acid detection due to the high surface area-to-weight ratio, and fast electron-transfer capabilities.[22] In this work, we tried to electrodeposit Au NPs on synthesized CNT–GS composites (named as Au@CNT–GS hybrids) and utilized the synergic effect in the electron transfer performance and biocompatibility of the resulting composites to modify the working electrode for immobilizing larger amounts of capture DNA probe CMV-F (S_1).

In this paper, we designed an ultrasensitive ECL biosensor for lengthy DNA molecules detection by employing Au@CNT–GS hybrids and CdTe–ZnO nanocomposites for dual signal amplification. Au@CNT–GS hybrids were introduced to modify GCE to increase the ECL signal and after S_1 was linked to the Au@CNT–GS hybrids, the electrode could be used as an ECL DNA biosensor. The resulting biosensor was applied to sandwich-type DNA bioassay using S_3 conjugated with CdTe–ZnO nanocomposites to amplify the ECL signal at lower potential with good stability. By coupling with the ECL analytical technique and proposed nanomaterials, the present biosensor showed excellent analytical performance for the ultrasensitive detection of lengthy DNA molecules.

2 Materials and methods

2.1 Reagents

All reagents were of analytical-reagent grade or the highest purity available and directly used for the following experiments. Aqueous solutions unless indicated were prepared with Milli-Q water (Millipore, USA). Hydrated zinc acetate ($Zn(CH_3COO)_2 \cdot 2H_2O$), chloroauric acid ($HAuCl_4 \cdot 4H_2O$) were obtained from Shanghai Chemical Reagent Company (Shanghai, China). CNTs were purchased from Nanoport. Co. Ltd. Thioglycolic acid (TGA), 3-aminopropyltriethoxysilane (ATPES), tris-(2-carboxyethyl)phosphine hydrochloride (TCEP), glutaraldehyde (GA), *N*-(3-dimethyl-aminopropyl)-*N*-ethyl-carbodiimide (EDC) and *N*-hydroxysuccinimide (NHS, 98%) were bought from Alfa Aesar China Ltd. 6-Mercapto-1-hexanol (MCH) was purchased from Nanoport. Co. Ltd. (Shenzhen, China).

The sequences of oligonucleotides are presented on the Table 1. Oligonucleotides S_1, S_3, S_4 and S_5 were synthesized and purified from Shanghai Linc-Bio Science Co. Ltd. (Shanghai, China). Lengthy DNA molecules (S_2) were kindly provided from Heng Liu (Qilu Hospital of Shandong University).

2.2 Apparatus

The ECL experiments were performed on MPI-B ECL analyzer (Remax, Xi'an) equipped with a PMT and a potentiostat at room temperature. Ultrasonic processing was performed on a JY92-IIDN ultrasonic apparatus (Ningbo Scientz biotechnology Co. Ltd., China). The photoluminescence (PL) spectra were obtained on a RF-5301 spectrofluorometer (P.C. Shimadzu, Japan). Scanning electron microscope (SEM) analyses were performed using a JSM-6700F microscope (JEOL, Japan), and the microscope was equipped with an Oxford X-MAX50 energy dispersive spectrometer (EDS) (Oxford, Britain). Transmission electron microscope (TEM) images were obtained from a JEOL JEM-1400 microscope (JEOL, Japan). Powder X-ray diffraction (XRD) patterns were collected on a Pa D8 advance diffractometer system equipped with Cu Kα radiation (Bruker Co., Germany). Electrochemical impedance spectra (EIS) were performed on a CHI 604D Electrochemical Workstation (Shanghai CH Instruments Inc., China).

2.3 Synthesis of GS and acid treatment of CNTs

Graphene oxide (GO) was synthesized from natural graphite powder using a modified Hummers and Offeman's method.[23] GS was prepared by the chemical reduction of GO using hydrazine as the reducing agent. Briefly, 15 mg of prepared GO was dispersed in Milli-Q water by ultrasonication. After that, 20 μL of hydrazine solution (80 wt%) and 100 μL of ammonia solution were added to the above homogeneous dispersion. The resulting solution was then stirred at 90 °C for 2 h.

CNTs were first carboxyl functionalized and shortened by sonicating in a mixture of concentrated HNO_3 and H_2SO_4 (v/v, 1 : 3) for 4 h followed by extensive washing in water until the filtrate was at neutral pH.[24] After this procedure, the CNTs were better separated and more active centers were formed in the surface. The acid-treated CNTs were dispersed into water.

2.4 Preparation of CdTe QDs coated hollow ZnO nanoparticles

First, for the preparation of hollow ZnO NPs, 1.098 g of ($Zn(CH_3COO)_2 \cdot 2H_2O$) was added to a beaker containing 23.5 mL of DMSO under stirring. Then, ultrasonication was performed on the mixture by an ultrasonic apparatus (Sonics: VCX-900W, 50% amplitude) for 30 min (15 s on and 5 s off) under ambient conditions. A white precipitate was centrifuged, washed with water and absolute ethanol in sequence, and finally dried in air. The final products were collected for characterization and further preparation.

To obtain CdTe–ZnO nanocomposites, we introduced the luminescent CdTe QDs (detail synthesis procedures in ESI†) by silylating the ZnO surface with APTES and then using the NH_3^+ groups to promote ionic interactions with negatively charged QDs. The detailed synthesis of CdTe–ZnO nanocomposites is described as follows. 0.5 g of the prepared ZnO NPs was first dispersed in 6 mL of ethanol and treated with 1.5 mL of APTES. After stirring for 6 h, the suspension was centrifuged and washed with ethanol for four times, to obtain amino-functionalized ZnO

Table 1 DNA sequences used in this work

Name	Sequence (5′–3′)	Length (nucleotides (nt))
Capture DNA, CMV-F (S_1)	NH_2-CGCA AATG GGCG GTAG GCGTG	21
Target DNA (S_2)	GCGTTTACCCGCCATCCGCAC…ATTATGCTGAGTGATATCC	5.7 K
Signal T7 promoter (S_3)	TAAT ACGA CTCA CTAT AGG-NH_2	19
Interfering DNA (S_4)	GCCGCTCACACGATATTTTTTTTGGATCGATCGTACGA	38
Interfering DNA (S_5)	ACTGCT AGAGATTTTCCACACTGACTAAAAGGGTCTGAG GGA	43

NPs. Then, amino-functionalized ZnO NPs were dispersed in a mixture of CdTe QDs (1.0 mL) and EDC (50 mM, 2.0 mL). The mixed suspension was stirred at 4 °C for 12 h. Unbound CdTe QDs were removed by successive centrifugation and washed with water several times. Finally, the as-prepared CdTe–ZnO nanocomposites were obtained and dispersed in water to a final volume of 3 mL.

2.5 Fabrication of the DNA sensor

A sandwich-type DNA sensing platform was constructed on a glassy carbon electrode (GCE) (3 mm diameter), as shown in Fig. 1. GCE was firstly polished with 1.0, 0.3 and 0.05 μm alumina powder respectively and rinsed thoroughly with ethanol and water in an ultrasonic bath, and dried in air at room temperature. Then, 5 μL of GS (1.0 mg mL^{-1}) was initially deposited on the electrode surface, and dried at room temperature. Subsequently, 5 μL of acid-treated CNTs (2 mg mL^{-1}) were cast on an electrode and dried under an infrared lamp. After that, AuNPs were electrodeposited on the CNT–GS-modified GCE surface by immersing the GCE into 3 mL of mixture solution of 1% $HAuCl_4$ and exerting the potential of −0.2 V for 30 s. The modified working electrode was immediately used for the preparation of DNA biosensor by immersing the electrode into an immobilization buffer containing 1.0×10^{-8} M capture probe DNA (S_1) for 40 min. The S_1 modified electrode was further treated with 1.0 mM MCH for 30 min to obtain a well-aligned DNA monolayer and block the uncovered electrode surface, followed by washing with water to remove physical adsorption. The as-prepared DNA biosensor (designed as MCH/S_1-Au@CNT–GS/GCE) was used for detection of target DNA (S_2). Part of this fabrication process of the ECL DNA biosensor is illustrated in Fig. 1. For the hybridization reaction, the modified electrode was immersed into stirred Tris–HCl solution containing target DNA (S_2) for 50 min at 42 °C allowing DNA strands to be stretched out well, which was an important procedure (before hybridization with the capture probe, the double-stranded DNA was denatured to single-stranded DNA by keeping the tube at 95 °C for 10 min and then in a freezing mixture consisting NaCl and ice for 1 min). The S_2-/MCH/S_1-Au@CNT–GS/GCE was secondly hybridized with signal probe loaded on CdTe–ZnO (CdTe–ZnO-S_3) (prepared by mixing CdTe–ZnO, GA, amino modified S_3) for 60 min at 42 °C. After hybridization, the electrode was extensively rinsed with washing buffer (10 mM Tris–HCl, pH ~ 7.8) and dried under a stream of nitrogen.

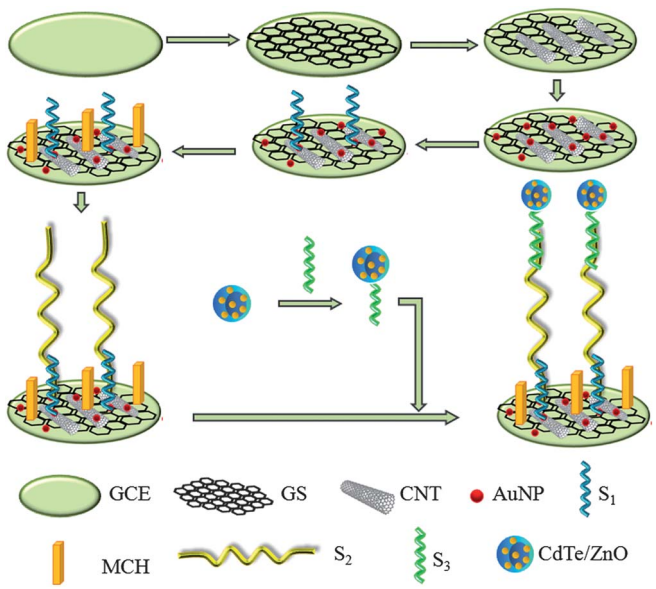

Fig. 1 Schematic representation of the fabrication of the ECL DNA biosensor.

2.6 ECL detection of target DNA

ECL measurements were carried out at room temperature and the potential swept from −1.56 to 0 V with scan rate of 100 mV s^{-1} in 2 mL of 10 mM Tris–HCl buffer solution (pH ~ 7.8) containing 0.05 M $K_2S_2O_8$ as the coreactant and 0.1 M KCl with a photomultiplier tube voltage of 800 V. The ECL signals related to the target DNA (S_2) concentrations could be measured.

3 Results and discussion

3.1 Characterization of GS, CNT–GS, and Au–CNT–GS

Fig. 2A shows a scanning electron microscope (SEM) image of the GS. It shows the deposition of petal-like graphene nanoflakes with lateral sizes of 400 nm, thin edges (with 10–20 nm thickness at the edges), and random directions, which all resulted in a large surface area. Fig. 2B shows SEM image of CNT–GS, and the distribution of fibrous CNTs on the surface of GS. When CNTs were cast on GS, the GS were hidden behind the CNTs and not so clear. GS and CNTs were used to accelerate electron-transfer capabilities. Fig. 2C shows SEM image of Au@CNT–GS composite. It was observed that AuNPs were deposited on the CNT–GS modified GCE uniformly with mean diameter of 10 nm.

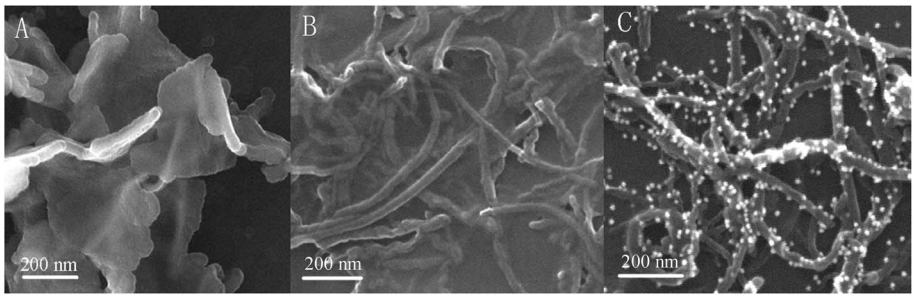

Fig. 2 SEM images of GS (A), CNT–GS (B) and Au@CNT–GS (C).

3.2 Characterization of CdTe–ZnO nanocomposite

As shown in Fig. 3A, the hollow ZnO NP with a diameter of about 100 nm was obtained successfully. Fig. 3B shows SEM image of CdTe–ZnO nanocomposite. Comparing with Fig. 3A and B, we can see that the surface texture of ZnO NPs changed after CdTe QDs were bonded to ZnO NPs. Fig. 3C shows yellowgreen emission from ZnO NPs and bright red emission from the CdTe–ZnO nanocomposites excited by an UV lamp, which confirmed that QDs were successfully connected to the ZnO NPs. EDS analysis of ZnO NP and CdTe–ZnO nanocomposite, respectively, further demonstrated the successful combination. It was observed that the elements Cd and Te existed in site "1" from Fig. 3E, but not in site "1" from Fig. 3D confirming the effective combination.

Photoluminescence spectra of CdTe QDs, ZnO NPs and CdTe–ZnO nanocomposites, respectively, are reported in Fig. 4A. As shown in Fig. 4, CdTe QDs showed an intense and broad band around at 633 nm, and ZnO NPs showed a weak and sharp emission at 570 nm, whereas CdTe–ZnO nanocomposites showed a relatively intense and broad band centered at 614 nm. According to the structural characteristics of the CdTe–ZnO nanocomposites, the emission band shift in the PL spectrum could be attributed to the interaction between the two semiconductors of CdTe and ZnO. The emission spectrum of CdTe–ZnO was dominated by an intense band at 633 nm, typical of CdTe nanocrystals, thus indicating that the presence of luminescent nanoentities allowed the modulation of the emission properties of ZnO NPs, and also indicated the successful preparation of CdTe–ZnO nanocomposites. Fig. 4B shows the X-ray diffraction (XRD) spectra taken from pure ZnO and CdTe–ZnO. For pure ZnO NPs, ten apparent diffraction peaks can be observed Fig. 4B. After combination of CdTe, three new peaks were observed in addition to the diffraction peaks from the ZnO NPs. These three broad peaks are centered at 23.96, 39.40, and 46.53°, which can be indexed, respectively, to the (111), (220), and (311) planes of the CdTe (JCPDS file no. 65-880). This confirmed the existence of CdTe QDs on ZnO NPs.

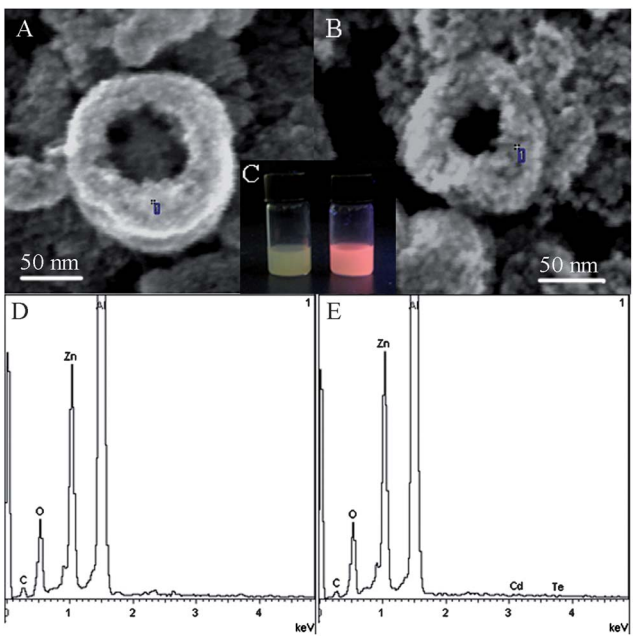

Fig. 3 SEM images of hollow ZnO NP (A) and CdTe–ZnO nanocomposite (B), photograph of ZnO NPs and CdTe–ZnO nanocomposites exposed to the UV lamp (C), EDS of ZnO NP (D) and CdTe–ZnO nanocomposite (E).

3.3 Possible mechanism for the ECL behaviors of the CdTe–ZnO nanocomposites

Nanocrystals can be reduced and oxidized by charge injection during potential cycling at the electrodes. ECL mechanism of the CdTe–ZnO system could be inferred from the ECL mechanism for CdTe QDs[25] and ZnO NPs[26] in the absence of the coreactant $K_2S_2O_8$.

Herein, ECL is based on the electron-transfer reaction between reduced species formed in CdTe–ZnO nanocomposite and oxidized species of the co-reactant (SO_4^{-}). $S_2O_8^{2-}$ is

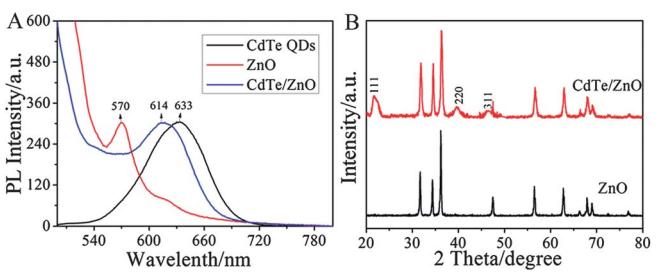

Fig. 4 PL spectra of CdTe QDs, ZnO NPs and CdTe–ZnO nanocomposites (A), XRD patterns of ZnO NPs and CdTe–ZnO nanocomposites (B).

reduced and generates a strong oxidant $SO_4^{-\cdot}$, then $SO_4^{-\cdot}$ reacts with the electrogenerated species ($CdTe–ZnO^{-\cdot}$) to generate higher intensity light emission. The corresponding ECL processes are expressed as follows:

$$CdTe–ZnO + e^- \rightarrow CdTe–ZnO^{-\cdot} \quad (1)$$

$$S_2O_8^{2-} + e^- \rightarrow SO_4^{2-} + SO_4^{-\cdot} \quad (2)$$

$$CdTe–ZnO^{-\cdot} + SO_4^{-\cdot} \rightarrow CdTe–ZnO^* + SO_4^{2-} \quad (3)$$

$$CdTe–ZnO^* \rightarrow CdTe–ZnO + h\nu \quad (4)$$

In order to identify the superiority of CdTe–ZnO nanocomposites, the cyclic voltammogram (CV) and ECL-potential curves for the CdTe–ZnO nanocomposites constructed sandwich-type DNA biosensor were measured in pH 7.8 Tris–HCl containing 0.05 M $K_2S_2O_8$ and 0.1 M KCl, as well as those of pure CdTe QDs and ZnO NPs as controls under the same conditions.

As shown in Fig. 5, the integral luminescence intensity was recorded simultaneously with the cathodic current as the potential was scanned in the negative direction. The CV curve of CdTe–ZnO nanocomposites showed reduction peaks at −0.82 V (Fig. 5A), which could be attributed to the reduction of CdTe–ZnO during the cathodic scanning. From Fig. 5B, the synthesized CdTe–ZnO nanocomposites showed an intensive ECL emission peak at −1.56 V, with an onset potential of −0.82 V that was consistent with the cathodic peak current position. Compared with pure CdTe QDs, it can be seen that the ECL intensity of CdTe–ZnO nanocomposites is 3-fold greater than that of pure CdTe QDs, and the ECL peak voltage is much more positive than that of pure CdTe QDs as well as the ECL onset voltage. Compared with ZnO NPs, about 2-fold magnitude enhanced ECL intensity for CdTe–ZnO nanocomposites was obtained, and the ECL peak voltage shifted positively from −1.60 V to −1.56 V though the ECL starting voltage shifted negatively a little. These improved properties can be ascribed to the more surface defects of the CdTe–ZnO nanocomposite, because ECL emission is dependent on the presence of surface defects to a large extent.[27,28] The obvious superiority of CdTe–ZnO nanocomposites was observed by the ECL efficiency being much higher and the ECL peak voltage lower than those of CdTe QDs and ZnO NPs.

3.4 EIS characterization of the DNA biosensor

EIS is an effective tool for probing the features of surface-modified and biomaterial-functionalized electrodes. Fig. 6A shows the Nyquist plots of EIS corresponding to the stepwise modification processes. For a bare GCE surface, the impedance spectrum (curve a) exhibited a small electron-transfer resistance (R_{et}). When GS (curve b), CNTs (curve c) and AuNPs (curve d) were modified on the GCE surface the resistance decreased accordingly. The big drop of impedance in curve d was owing to the synergy of GS and CNT which can greatly enhance electron transfer. However, the R_{et} increased (curve e) after S_1 was covalently immobilized on the modified GCE. Then, MCH (curve f), target DNA S_2 (curve g) and CdTe–ZnO-S_3 (curve h) were constructed step by step, and the R_{et} of each related electrode increased correspondingly. The reason for the resistance increase was that nonconductive properties of a biomacromolecule obstruct electron transfer and mass transport of the electrochemical probe. The EIS results indicated that the biomacromolecules were successfully assembled on the electrode surface.

We assembled CNTs on graphene to obtain the synergic effect in the electron transfer performance, and the improved performance was shown in Fig. 6B. It was observed that the fabricated biosensors showed similar ECL intensity when graphene (curve a) or CNT (curve b) was assembled on GCE. A greatly enhanced ECL performance was obtained when CNT–GS was applied to modify GCE. The inset showed plots of ECL intensity of the biosensor *vs.* target DNA concentration for Au@GS, Au@CNT and Au@CNT–GS modified GCE, respectively. From the inset, it can be seen that the CNT–GS could be chosen to fabricate biosensor, due to their synergic effect in electron transfer performance.

3.5 Sensitive detection of target DNA

Under the optimal conditions (see ESI†), the ECL intensities for the Au@CNT–GS-based sensor after hybridization with different concentrations of target DNA (S_2) are shown in Fig. 7. As shown in Fig. 7, the signal increased with increasing the concentration of the target DNA. In particular, we found that the assay was still responsive with 10^{-19} M target DNA. The inset was the calibration curve for the determination of S_2. It was found that the response signal was logarithmically proportional to the

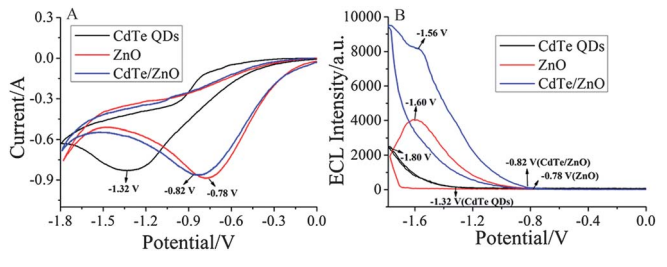

Fig. 5 Cyclic voltammograms (A) and ECL-potential curves (B) of CdTe QDs, ZnO NPs and CdTe–ZnO nanocomposites in pH 7.8 Tris–HCl containing 0.05 M $K_2S_2O_8$ and 0.1 M KCl.

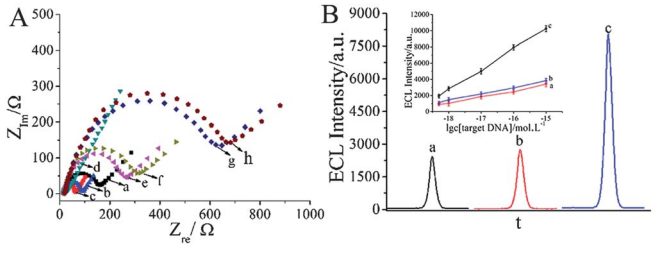

Fig. 6 EIS of the modified GCE in 5.0 mmol L^{-1} $K_3Fe(CN)_6$ containing 0.1 mol L^{-1} KCl (A), ECL profiles of DNA biosensor using Au@GS (curve a), Au@CNT (curve b) and Au@CNT–GS (curve c) modified GCE in 10 mM Tris–HCl buffer (pH 7.8) containing 0.05 M $K_2S_2O_8$ and 0.1 M KCl (B).

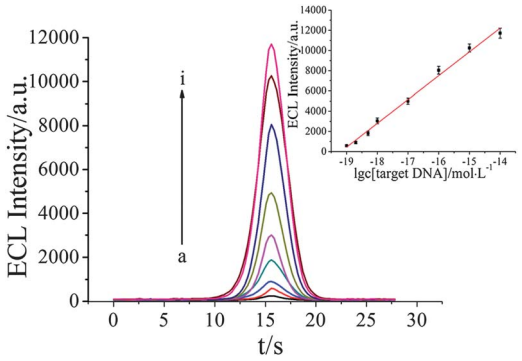

Fig. 7 ECL profiles of the DNA biosensor in the presence (a–i) of different concentrations of S_2 in 10 mM Tris–HCl buffer (pH 7.8) containing 0.05 M $K_2S_2O_8$ and 0.1 M KCl. S_2 concentration (M): (a) 0, (b) 10^{-19}, (c) 2×10^{-19}, (d) 5×10^{-19}, (e) 10^{-18}, (f) 10^{-17}, (g) 10^{-16}, (h) 10^{-15}, (i) 10^{-14} (the voltage of the photomultiplier tube was set at 800 V). Inset is the calibration curve of the DNA biosensor.

target concentration in the range from 10^{-14} M to 10^{-19} M, and the equation of linear regression was $\Delta ECL = 45210.87 + 2374.13 \lg c_{DNA}$ (mol L^{-1}), with a correlation coefficient of 0.9902. A detection limit of 0.61×10^{-19} M target DNA can be estimated at a signal-to-noise of 3 criterion. The use of our Au@CNT–GS and CdTe–ZnO indicated that the detection limit had improved to a greater extent compared with other methods. As shown in Table 2, our strategy was more sensitive than those of nanoparticle, nanotube, conductive polymer, and other nanostructure-modified assay as reported previously.

3.6 Regeneration, reproducibility, stability and specificity of the DNA biosensor

Regeneration is an extremely important feature for biosensors in practical applications such as clinical diagnoses. In our test, the DNA biosensor could be regenerated by incubation of the modified electrode in hot water (95 °C) for 3 min, by which hybridized DNA was removed *via* thermal denaturation. As shown in Fig. S2 (see ESI†), the as-renewed electrode could restore 88.2%, and 91.3% of the initial value for unheated modified electrode at target DNA concentrations of 10^{-16} M and 10^{-17} M.

Reproducibility of the DNA biosensor for target DNA was investigated with intra- and interassay precision. The interassay precision was evaluated by assaying one target DNA level for five similar measurements. The interassay precision was estimated by testing one target DNA level with five DNA biosensors made at the same electrode independently. The intra- and interassay variation coefficients obtained from 1.0×10^{-16} M were 5.1% and 6.3%, respectively. This fact demonstrated the DNA biosensor possessed acceptable reproducibility.

The stability is a vital parameter in the performance of the prepared DNA biosensor. As shown in Fig. S3 (see ESI†), after running for 15 cycles, only a 2.6% decline of the original ECL was observed, which demonstrated that the sensing layer of the DNA biosensor owned excellent stability. In addition, as shown in Fig. S4 (see ESI†) after the DNA biosensors were stored in pH 7.8 Tris–HCl at 4 °C for two weeks, the ECL signal declined 3.08% and 3.26% of the immediate value for the prepared biosensor at target DNA concentrations of 10^{-16} M and 10^{-17} M, respectively. This result indicates that the DNA biosensor had good stability.

The specificity of the proposed DNA assay was also investigated by using different DNA strands (S_4 and S_5) as interfering analytes. The target DNA S_2 and interfering strands S_4 and S_5 were detected both at a concentration of 10^{-16} M. The ECL responses to each DNA strand and the mixed DNA strands were recorded in Fig. S5.† As shown in Fig. S5,† the signals from S_4 and S_5 solutions were no different from the blank, and the ECL responses of mixed DNA strands showed no obvious change compared with pure S_2. These results indicated that this proposed DNA assay owned excellent specificity to distinguish it from other DNA targets.

4 Conclusions

In conclusion, we have demonstrated an ultrasensitive ECL sandwich-type strategy for the detection of lengthy DNA based on Au@CNT–GS composite and CdTe–ZnO nanocomposite. In this approach, the CdTe–ZnO labeled signal probe was used to selectively detect the target DNA while Au@CNT–GS was used to facilitate the efficient immobilization of the capture probes. The main advantages of the present biosensor contribute to several aspects: (1) Target DNA in this work contains 5.7 thousand base pairs, which are about as many as the base pairs contained in the DNA existing in some organisms and seldom researched in previous reports. (2) The proposed strategy which based on CdTe–ZnO nanocomposites greatly amplifies the ECL signal and

Table 2 Comparison between the proposed assay and other reported techniques for the determination of DNA hybridization

Label or indicator	Analytical techniques	Detection limit of target DNA	References
Multiwalled carbon nanotubes	ac impedance	10 nM	29
Poly(pyrrole-*co*-3-pyrrolylacrylic acid)	Electrochemical impedance spectroscopy	0.98 nM	30
AuNPs with Ag amplification	Electrical detection	500 fM	31
Tin oxide nanoparticle	Photoelectrochemical detection	0.18 nM	32
Liposome	Liposome-amplified electrochemical detection	50 fM	33
NanoCuS tags	Flow injection chemiluminescence	0.55 pM	34
PdCu–CNCs composites	Electrochemiluminescence	18 aM	35
Au nanoparticles dotted CNTs–GS and CdTe–ZnO composite	Electrochemiluminescence	0.1 aM	This work

allows the sensitive detection at lower applied potential. (3) The ECL sensing platform that was constructed with Au@CNT–GS composite makes a good contribution to the high ECL efficiency. (4) The biosensor can detect levels as low as 0.61×10^{-19} M target DNA, which is superior to other methods. These features, as well as its other advantages, such as good stability, excellent biocompatibility and low cost, make it a promising candidate for biomedical and bioanalytical applications requiring high-performance genetic or proteins target analysis.

Acknowledgements

This work was financially supported by Technology Development Plan of Shandong Province, China (Grant no. 2011GGB01153), Natural Science Research Foundation of China (no. 21175058) and Natural Science Foundation of Shandong Province, China (ZR2011BQ019).

References

1 J. Huang, Y. R. Wu, Y. Chen, Z. Zhu, X. H. Yang, C. Y. J. Yang, K. M. Wang and W. H. Tan, *Angew. Chem., Int. Ed.*, 2011, **50**, 401.
2 S. Bi, J. L. Zhang and S. S. Zhang, *Chem. Commun.*, 2010, **46**, 5509.
3 K. C. Hu, D. X. Lan, X. M. Li and S. S. Zhang, *Anal. Chem.*, 2008, **80**, 9124.
4 J. H. Chen, J. Zhang, J. Li, F. F. Fu, H. H. Yang and G. N. Chen, *Chem. Commun.*, 2010, **46**, 5939.
5 B. T. Zhang, L. H. Guo and M. M. Greenberg, *Anal. Chem.*, 2012, **84**, 6048.
6 X. Liu, L. X. Cheng, J. P. Lei and H. X. Ju, *Analyst*, 2008, **133**, 1161.
7 G. F. Jie, B. Liu, H. C. Pan, J. J. Zhu and H. Y. Chen, *Anal. Chem.*, 2007, **79**, 5574.
8 G. Z. Zou, H. X. Ju, W. P. Ding and H. Y. Chen, *J. Electroanal. Chem.*, 2005, **579**, 175.
9 D. J. Lin, J. Wu, M. Wang, F. Yan and H. X. Ju, *Anal. Chem.*, 2012, **84**, 3662.
10 D. Y. Liu, Y. Y. Xin, X. W. He and X. B. Yin, *Analyst*, 2011, **136**, 479.
11 J. Zhang, H. L. Qi, Y. Li, J. Yang, Q. Gao and C. X. Zhang, *Anal. Chem.*, 2008, **80**, 2888.
12 J. Geng, X. D. Jia and J. J. Zhu, *CrystEngComm*, 2011, **13**, 193.
13 V. Mani, B. V. Chikkaveeraiah, V. Patel, J. S. Gutkind and J. F. Rusling, *ACS Nano*, 2009, **3**, 585.
14 J. Wang, G. Liu and M. R. Jan, *J. Am. Chem. Soc.*, 2004, **126**, 3010.
15 D. Du, Z. X. Zou, Y. Shin, J. Wang, H. Wu, M. H. Engelhard, J. Liu, A. A. Ilhan and Y. H. Lin, *Anal. Chem.*, 2010, **82**, 2989.
16 R. J. Cui, H. P. Huang, Z. Z. Yin, D. Gao and J. J. Zhu, *Biosens. Bioelectron.*, 2008, **23**, 1666.
17 C. Lee, X. Wei, J. W. Kysar and J. Hone, *Science*, 2008, **321**, 385.
18 A. A. Balandin, S. Ghosh, W. Bao, I. Calizo, D. Teweldebrhan, F. Miao and C. N. Lau, *Nano Lett.*, 2008, **8**, 902.
19 J. C. Meyer, A. K. Geim, M. I. Katsnelson, K. S. Novoselov, T. J. Booth and S. Roth, *Nature*, 2007, **446**, 60.
20 S. Park and R. S. Ruoff, *Nat. Nanotechnol.*, 2009, **4**, 217.
21 J. Wang, H. Y. Han, X. C. Jiang, L. Huang, L. N. Chen and N. Li, *Anal. Chem.*, 2012, **84**, 4893.
22 D. Kauffman, D. Sorescu, D. Schofield, B. Allen, K. Jordan and A. Star, *Nano Lett.*, 2010, **10**, 958.
23 W. S. Hummers and R. E. Offeman, *J. Am. Chem. Soc.*, 1958, **80**, 1339.
24 D. R. S. Jeykumari and S. S. Narayman, *Biosens. Bioelectron.*, 2008, **23**, 1404.
25 J. Qian, C. Y. Zhang, X. D. Cao and S. Q. Liu, *Anal. Chem.*, 2010, **82**, 6422.
26 R. X. Zhang, L. Z. Fan, Y. P. Fang and S. H. Yang, *J. Mater. Chem.*, 2008, **18**, 4964.
27 Z. Ding, B. M. Quinn, S. K. Haram, L. E. Pell, B. A. Korgel and A. J. Bard, *Science*, 2002, **296**, 1293.
28 N. Myung, Y. Bae and A. J. Bard, *Nano Lett.*, 2003, **3**, 1053.
29 H. Cai, Y. Xu, P. He and Y. Fang, *Electroanalysis*, 2003, **15**, 1864.
30 H. Peng, C. Soeller, N. Vigar, V. Caprio and J. Travas-Sejdic, *Biosens. Bioelectron.*, 2007, **22**, 1868.
31 S. J. Park, T. A. Taton and C. A. Mirkin, *Science*, 2002, **295**, 1503.
32 S. Liu, C. Li, J. Cheng and Y. Zhou, *Anal. Chem.*, 2006, **78**, 4722.
33 F. Patolsky, A. Lichtenstein and I. Willner, *Angew. Chem., Int. Ed.*, 2000, **39**, 940.
34 C. F. Ding, H. Zhong and S. S. Zhang, *Biosens. Bioelectron.*, 2008, **23**, 1314.
35 M. Yan, M. Zhang, S. G. Ge, J. H. Yu and M. Li, *Analyst*, 2012, **137**, 3314.